Nano Energy 74 (2020) 104864

Contents lists available at ScienceDirect

Nano Energy

journal homepage: http://www.elsevier.com/locate/nanoen

The role of anions on the Helmholtz Plane for the solid-liquid interface in aqueous rechargeable lithium batteries

Jiangtao Hu [1], Wenju Ren [1], Xin Chen [1], Yiwei Li, Weiyuan Huang, Kai Yang, Luyi Yang, Yuan Lin [**], Jiaxin Zheng [***], Feng Pan [*]

School of Advanced Materials, Peking University, Shenzhen Graduate School, Shenzhen, 518055, China

ARTICLE INFO

Keywords:
Solid-liquid interface
Helmholtz plane
$LiFePO_4$
Aqueous rechargeable lithium batteries

ABSTRACT

The Li-ion transport at the electrode/electrolyte interface in lithium ion batteries (LIBs) relies on the structure of the electrical double layer. Our previous work indicates that the constructing of Janus amphiphilic coordination interface on $LiFePO_4$ in aqueous electrolyte relieves the energy barriers of the Li^+ solvation/desolvation process. Here, aqueous electrolytes with different salts ($LiNO_3$, LiCl, Li_2SO_4 and CH_3COOLi) were tested in $LiFePO_4$ single nanoparticle, and Ab initio calculations and simulation were carried out. H_2O has a stronger binding energy with Fe and Li on the surface of $LiFePO_4$ to form Janus interface, so the activation energies of Li-ion in Janus layer are the same in the four electrolytes. The simulation result confirms that the Li-ion transport at the interface have a close relationship with the anionic physical characteristics. Combing with the experimental and calculated results, it can be inferred that the activation energy (E_a) of Li-ion includes Janus interface, anion adsorption layer and cation adsorption layer. Owing to the same Janus interface and cation adsorption layer, the difference of E_a in the four kinds of electrolytes must come from the anion adsorption layer in inner Helmholtz plane (IHP). This work provides a guiding significance on development of aqueous electrolyte systems.

1. Introduction

Incented by the ever-increasing demands of advanced energy storage systems for portable electronic devices and electric vehicles (EVs), the development of high-performance cathode materials for lithium ion batteries (LIBs) has attracted worldwide attentions. Consequently, the electrochemical properties and mechanisms of cathode materials have been extensively studied in the past decade. While most current studies in this area mainly focus on the macroscopic bulk crystal structure and properties, other previous studies suggest that the interfacial structures of materials largely dictates their electrochemical performances due to their unique electrical double layer formed at different chemical/electrochemical conditions. Electrical double layer (EDL) is always existence on electrode/electrolyte interface as an essential constituent, no matter whether there is solid electrolyte interphase (SEI) or not [1,2]. Helmholtz is one kind of the classical models in EDL, which includes inner Helmholtz plane (IHP) and outer Helmholtz plane (OHP). In general, adsorbed ions or molecules are located in IHP and solvated adsorbed ions belongs to OHP [3]. The thin Helmholtz plane has a big influence on electrochemical performance, such as capacitor and LIBs, which has attracted a lot of attentions [4]. For example, Yan et al. investigated different adsorption species in IHP of Li-metal, which has great influence on diffusion of Li-ion from electrolyte to Li-metal surface [5]. Wang and Xu's group achieved high working voltage and improved cycle ability in aqueous Li-ion batteries by building a stable protecting layer on IHP [6,7].

Our recent work found that replacing traditional organic electrolytes with aqueous electrolytes leads to different kinetics for ion intercalation and de-intercalation for $LiFePO_4$ LIBs [8,9]. By combining theoretical simulations with electrochemical characterization techniques in atomic/nano scales such as single-particle and mass-electrochemical measurements, microscopic information of the solid-liquid interfacial reactions has been obtained [10]. We found that the FeO_6 and LiO_6 octahedral structure units in crystal were symmetrically broken to

* Corresponding author.
** Corresponding author.
*** Corresponding author.
E-mail addresses: linyuan@iccas.ac.cn (Y. Lin), zhengjx@pkusz.edu.cn (J. Zheng), panfeng@pkusz.edu.cn (F. Pan).
[1] These authors contributed equally to this work.

https://doi.org/10.1016/j.nanoen.2020.104864
Received 11 January 2020; Received in revised form 18 April 2020; Accepted 19 April 2020
Available online 28 April 2020

become FeO_5 and LiO_3 units at surface, which interacted with solvent H_2O molecule to create both $FeO_5(H_2O)$ and $LiO_3(H_2O)_3$ octahedral reconstructive structure units (named as a "Janus" interface) at the EDL that relieves the energy barriers of the Li^+ solvation/desolvation process, ultrafast rate performances can be achieved. At this point, one question has been aroused: what's the role of anions on the formation of EDL in the aqueous electrolytes? Owing to the high structural stability and relatively low operating voltages, the surfaces of olivine materials are immune to side reactions compared to other cathode materials, such as Ni-rich layered cathode materials [11,12]. Though the final cathode material is covered by a thin carbon layer for high electronic conductivity, which has a loose structure with a large number of internal spaces, so the water molecules can permeate the carbon coat [9,13]. Therefore, the $LiFePO_4$ system is still an ideal model to reveal the impact of anions on the interfacial properties of cathode materials [14].

In this work, we improved our previous single particle (SP) model to deal with a wider temperature scope to explore the role of anions in aqueous electrolytes. The quasi single particle (QSP) electrode of $LiFePO_4$ was tested in different electrolytes (1 M $LiNO_3$, 1 M LiCl, 0.5 M Li_2SO_4 and 1 M CH_3COOLi) and different temperatures (0, 25 and 50 °C). By simulation and comparing the cyclic voltammogram (CV) curves of the four kinds of electrolytes, we found that the standard rate constant (k^0) for Li-ion intercalation and de-intercalation inter has a strong relationship with the ionic radius: the bigger of ionic radius, the smaller of k^0 value. Moreover, the interaction between anion and Li-ion is also important for Li-ion transport, such as CH_3COOLi, which owns the shortest radius but the transfer speed of Li-ion is slower compared with $LiNO_3$ and LiCl owning to the strong interaction between CH_3COO^- and Li-ion. By ab initio calculations, we proved that not only H_2O, but also the anions can realize interface reconstruction and form octahedral structure in vacuum condition, but H_2O has priority in the real liquid environment. In aqueous electrolytes, anions will be absorbed next to the Janus $LiFePO_4/H_2O$ inner Helmholtz plane (IHP) by electrostatic interaction, and the thickness of absorbed layer (d value) has a great influence on Li-ion transport between electrolyte and active materials. Finally, we separated the above four kinds of electrolytes into two group: fast-type electrolytes ($LiNO_3$ and LiCl) and slow-type (Li_2SO_4, CH_3COOLi), the former group owns smaller activation energy and little pre-exponential factor, which is beneficial for Li-ion transport between electrolyte and active material.

2. Experimental methods

2.1. Preparation of $LiFePO_4$@C

The $LiFePO_4$ nanocrystals were synthesized by the normal method, mixing $FeSO_4.7H_2O$ (AR, 99%), H_3PO_4 (AR, 85% solution) and LiOH. H_2O (AR, 95%) in ethylene glycol (AR, 99%) according to a specific proportion, and the detailed processes are presented in our previous work [8].

2.2. Characterization

The crystal structure data of $LiFePO_4$@C was collected by X-ray diffraction (XRD, Bruker D8 Advance diffractometer with a Cu-Ka radiation source). The morphology of $LiFePO_4$@C was investigated by a scanning electron microscopy (SEM, ZEISS SURPA 55).

2.3. QSP electrode preparation, and electrochemical measurements

Three electrode measurement was carried out to make clear the influence of anions on lithium ion interfacial transport. The working electrode was made up by mixing $LiFePO_4$ nanocrystals (9 mg), carbon nano tube (6 mg), and Nafion solution (0.15 g, 5% concentration) into NMP (1.0 g) and ultrasound for a long time (more than 70 min). 60% PTFE solution is another binder used in our experiment. The final slurry was dropped on the quartz monitor crystals and dried by air dry oven, then the working electrode formed, which was named as quasi single particle electrode (QSP electrode). The Ag/AgCl and platinum electrode were used as reference electrode and counter electrode, respectively. Then, we chose different salt dissolving in H_2O as the electrolyte, including 1 M $LiNO_3$, 1 M LiCl, 0.5 M Li_2SO_4 and 1 M CH_3COOLi. Finally, the electrochemical performance of $LiFePO_4$ QSP electrode measured in different electrolytes were collected by cyclic voltammetry (CV) measurements recorded by a CHI electrochemistry workstation (CHI604E).

2.4. Calculation method

All calculation was performed using the first-principles density functional theory (DFT) calculations with the exchange–correlation energy functional, which were described by a generalized gradient approximation with the Perdew–Burke–Ernzerhof (PBE) exchange–correlation function [15]. To simulate H_2O, Cl^-, NO_3^- and SO_4^{2-} absorbed on the $FePO_4$ and $LiFePO_4$ (0 1 0) surfaces, two ($1 \times 1 \times 3$) supercell were used and enabled by a VASP code in which the projector augmented wave (PAW) method represented the electron–ion interaction with a kinetic energy cutoff of 520 eV [16,17]. The k-points were $4 \times 2 \times 1$ for the supercell using the Monkhorst–Pack method [18]. During optimizations, the energy and force converged to 10^{-4} eV per atom and 0.01 eV $Å^{-1}$, respectively. The spin = 2 polarization was used in all the calculations.

3. Results and disscussion

3.1. Section I. Experimental results

The XRD pattern of $LiFePO_4$ was collected, and all the diffraction peaks are fully indexed to the orthorhombic structure with Pnma(62) space group, consistent well with the standard peaks (JCPDS NO. 81–1173) as shown in Fig. 1a. Obviously, the final material is in pure phase without any impurity. According to our synthesis conditions (low temperature and reduction reaction environment) and some relevant works [19,20], the tiny amount of Fe_2P and FeOx impurities can be excluded. Combining with Scherrer equation $D = K\lambda/\beta\cos\theta$ (K is a dimensionless shape factor, λ is the XRD wavelength, β is the line broadening at half the maximum intensity (FWHM), θ is the Bragg angle) and the strongest peak (311), the mean particle size of $LiFePO_4$ was calculated to be about 46.22 nm. Fig. S1 shows the SEM images of $LiFePO_4$ with a mean size about 40–50 nm, consistent with the calculated results by Scherrer equation. We scattered the $LiFePO_4$ nano-particles in carbon nanotube (CNT) network, and treat it with ultrasonic by a long time (longer than 70 min). The detailed experimental process can be found in our previous work [8]. The above slurry was dropped on the quartz monitor crystals and dried in the air dry oven, which was named as quasi single particle (QSP) electrode. Fig. 1b shows the distribution situation of $LiFePO_4$ nano-particles and CNT on the QSP electrode, obviously, the $LiFePO_4$ particles were completely dispersed into the NCT network, which can minimize the concentration polarization, electrochemical polarization, and other internal interference.

It's well known that impurity phase (especially for Fe_2P) is easy to be generated during synthesis of $LiFePO_4$ [21,22], which can be easily detected by XRD and TEM. Thus, TEM measurements were performed to detect the possibility of impurity phase on the surface of our synthesized $LiFePO_4$. As shown in Figs. S2a and S2b, there is no signal of the existence of impurity phase on the $LiFePO_4$ particle surface, consistent with our XRD results and our previous work (Figs. S2c and S2d) [23]. This indicates the clean surface of our material. Previous works using the same synthesis method as ours also reported that no relevant impurities were detected [24,25]. For example, the work by William's group studied Li-ion diffusion on the surface of $LiFePO_4$ in aqueous electrolyte [14] and showed the same surface structure of $LiFePO_4$ as we did, and no

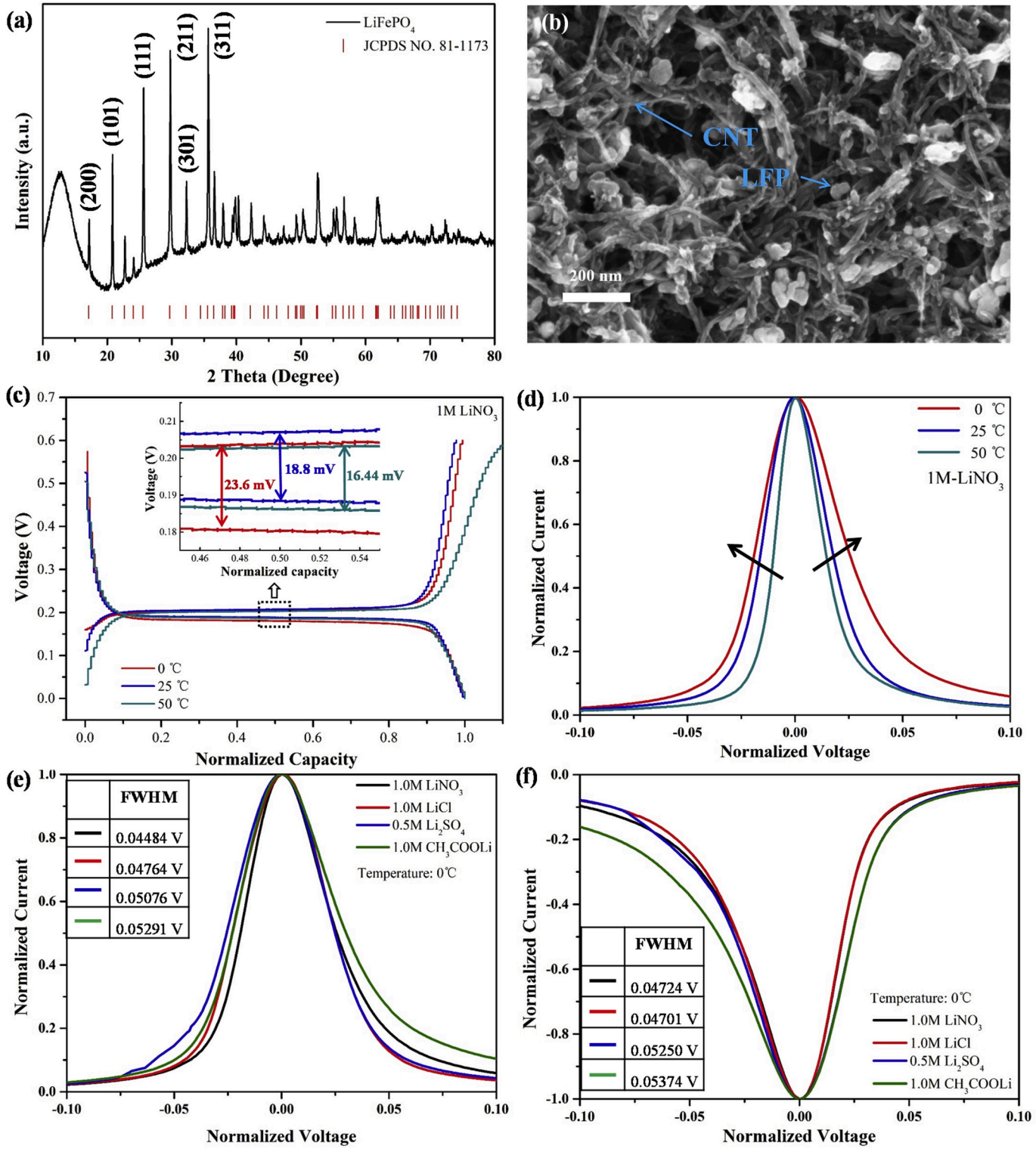

Fig. 1. (a) The XRD data of $LiFePO_4$. (b) SEM image of the QSP electrode, obviously, the electrode materials scattered very well in the CNT network. (c) Charge-discharge curves of the QSP electrode in 1 M $LiNO_3$ at different temperature at 0.1C, the inserted picture is partial enlarged detail of c, which shows us the polarization voltage in different temperature. (d) The normalized CV curves of the $LiFePO_4$ QSP electrode measured in 1 M $LiNO_3$. (e and f) The difference of normalized CV curves measured in different electrolytes at 0 °C, the Full Width at Half Maximum (HWHM) data of each curves are listed and inserted into (e) and (f).

impurity phases was detected on the facet other than the coated carbon.

Charge-discharge curves of $LiFePO_4$ in different electrolytes and temperatures were collected and shown in Fig. 1c and **S3**. The corresponding voltage interval and current density are 0–0.6 V and 0.1 C. As for 1 M $LiNO_3$, the voltage difference between charge-discharge platforms changed by a little content from 0 °C to 50 °C, which are 20.9 mV (0 °C), 17 mV (25 °C) and 16.9 mV (50 °C) (Fig. 1c). Under a certain condition, high temperature is helpful for Li-ion diffusion both in material and electrolyte, so the polarization phenomenon (platform difference) is weakened. $LiFePO_4$ tested in 1 M LiCl, 0.5 M Li_2SO_4 and 1

M CH_3COOLi also owns the same phenomenon, as shown in Fig. S3. Furthermore, cyclic voltammetry (CV) measurements were carried out in the above four kinds of electrolytes under different temperatures. Fig. 1d, **S4** and **S5** presents the normalized CV curves both in charge and discharge processes, which become narrower with the increase of temperature. For $LiNO_3$ electrolyte, the normalized FWHMs of the CV curves are 0.045V, 0.034V, and 0.0225V from 0 °C to 50 °C (Fig. 1d). In order to compare the differences of Li-ion transport in different electrolytes and different temperatures, we put the CV curves measured at the same temperature together and carried out normalization, as shown in Fig. 1e, f and S6. When tested at 0 °C, the FWHMs of CV curves in different electrolytes are different, and the peak of 1 M LiCl and 1 M $LiNO_3$ are the narrowest. The FWHMs of normalized CV curves during charge processes are 0.04484V ($LiNO_3$), 0.04764V (LiCl), 0.05076V (Li_2SO_4) and 0.05291V (CH_3COOLi), and the corresponding FWHMs during discharge processes are 0.04724V, 0.04701V, 0.05250V and 0.05374V (Table inserted into Fig. 1e and f). When the testing temperature increased to 50 °C, the difference of FWHMs are not so big compared with it tested in 0 °C, but CV curves are always the narrowest in LiCl and $LiNO_3$ (Figs. S6c and S6d). To exclude the affection of binder, we also prepared QSP $LiFePO_4$ electrode with PTFE binder. The new QSP electrode presents the same trends compared with the QSP electrode with Nafion binder (Fig. S7). Interestingly, with the same solution concentration and temperature, why CV curves show different FWHMs in aqueous electrolytes with different salts? With the same electrodes (working, counter and reference) used in all test systems, electrolytes are the only difference during the electrochemical tests. To clarify the reason accounting for the polarization difference, ionic conductivities of the four kinds of salts in H_2O were measured (Fig. S8). The corresponding conductivities of $LiNO_3$, LiCl, Li_2SO_4 and CH_3COOLi are 69, 74.18, 50.16 and 32.73 mS/cm at 25 °C, respectively. Obviously, the ionic conductivities of the four electrolytes are super higher than that in $LiFePO_4$ bulk with 10^{-9} S/cm [26], so the ionic conductivities in the electrolyte should not be the decisive step. Thus, the polarization difference must come from the different solid-liquid interfaces (Helmholtz layer) formed between $LiFePO_4$ and different aqueous electrolytes. Moreover, The Li^+ transference numbers (t) of 1 M $LiNO_3$, LiCl, Li_2SO_4 and CH_3COOLi aqueous electrolytes were calculated as shown in Fig. S8.

3.2. Section II. SP model and simulation results

We further performed electrochemical simulations to support the above inference. As we all know, Butler–Volmer (BV) model was usually selected to simulate and analyze the CV curves to get the transfer mechanism. However, it failed when used in two phase $LiFePO_4$ system [8]. However, in our previous model, a hypothesis was set that the whole Li-ion transfer processes would not stop in transitive state (Li_xFePO_4), owing to the fast transfer reaction between $LiFePO_4$ and $FePO_4$. That's to say, there are only two phase transformation in the whole processes. However, we found that the CV peak become wider under aqueous electrolyte in low temperature, and the old model failed to simulate the CV curves in which the interfacial reaction would be influenced by temperature. This can be attributed to the different transport characteristics of lithium ion at solid-liquid interface from that of our previous electrochemical systems. The different transport characteristic brought new transitive state, which is different with the previous Li-ion transport behavior. When the testing condition was changed (e. g., temperature), the previous model will be unsuitable in low temperature because transitive phase appears and cannot be ignored. It's necessary to develop an innovative and reasonable model to realize more smart simulation to fit widely various conditions.

First, we know that the charge-discharge process of $LiFePO_4$ is a partially dissoluble two-phase process as shown in the following equation:

$$LiFePO_4 - x\,Li - x\,e \leftrightarrow (1-x)\,LiFePO_4 + (x)\;\; FePO_4 \tag{1}$$

Note that the reaction rate is directly proportional to the surface concentration of $FePO_4$ and $LiFePO_4$. Define the concentration of $LiFePO_4$ and $FePO_4$ at the surface are $C_O(0, t)$ and $C_R(0, t)$. Then the current is determined by the rate of the reactant transmitted to the electrode surface. The net current of the whole reaction is:

$$\mathrm{i} = nFA'\left[k_f C_O(0,t) - k_b(C_R(0,t))\right] \tag{2}$$

(k_f is the heterogeneous reduction rate constant, k_b is the heterogeneous oxidation rate constant, F is Faraday constant, n is quantity of exchange electron, A' is specific interfacial surface area.)

The rate constant at different potential can be represented by the standard heterogeneous rate constant k^0, such as equations (3) and (4).

$$k_f = k^0 \exp\left[-aF/_{RT}\,(E - E^{\theta'})\right] \tag{3}$$

$$k_b = k^0 \exp\left[(1-a)F/_{RT}\,(E - E^{\theta'})\right] \tag{4}$$

The novelty of the modified SP model is that the Li-ion de-intercalation/intercalation process of $LiFePO_4/FePO_4$ was divided into three stages according to the charge/discharge curves (taking discharge as an example, as shown in Fig. 2a). The first stage is the high voltage part (Part I in Fig. 2a), which contains a small amount of Li-ion in $FePO_4$ (Li_xFePO_4; $0 < x < b$, $b \approx 0.1$). In this stage, we assume that k^0 remain the same, k_f and k_b is calculated by $FePO_4$ using equations (3) and (4). The second stage is two phase coexistence stage ($FePO_4$ & $LiFePO_4$; $b \approx 0.1$, $B \approx 0.9$), the value of b and B can be determined from the inflection point of the charge-discharge curve (Part II in Fig. 2a), and k_f and k_b are calculated according to the mixed value of $LiFePO_4$ and $FePO_4$. In order to describe the process, we set a formal potential E, which presents the activation energy voltage. To get the formal potential (E), which is a parameter that need to be identified, we first get the formal potential at the first stage (E_L) and the third stage (E_H), and then get the k_f and k_b in the second stage using the following equations (5) and (6).

$$k_f = k^0 \exp\left[(-\alpha)F/_{RT}\left(V(E - E_H + E_L)/_E - E_L\right)\right] \tag{5}$$

$$k_b = k^0 \exp\left[(1-\alpha)F/_{RT}\left(V(E - E_H + E_L)/_E - E_L\right)\right] \tag{6}$$

V is the scan voltage in the second stage.

The third stage is $LiFePO_4$ with some lithium vacancies (Li_xFePO_4; $B < x < 1$). In this stage, we assume that k^0 remain the same, k_f and k_b is calculated by $FePO_4$ using equations (3) and (4).

In the new model, lithium transport process as was divided in two parts, the diffusion process and interface charge transfer process. During the oxidation or reduction process, the Li-ions in $LiFePO_4$ will diffuse along the transport channel, and the diffusion process satisfies the diffusion law in spherical particle, as shown in Equation (7).

$$\frac{\partial C}{\partial t} = D_{Li}\frac{\partial^2 C}{\partial r^2} + 2\frac{D_{Li}}{r}\frac{\partial C}{\partial r} \tag{7}$$

D_{Li} is the diffusion coefficient of Li-ion, r is the radius of the nano $LiFePO_4$ particle.

Equation (3) and (4) can be brought into equation (2) to obtain the complete current (i)-electric potential (E) relation expression. The interface electron exchange process of QSP electrode is described by the following equation.

$$\mathrm{i} = \mathrm{FA'}k^0\left[C_O(0,t)e^{-\alpha f(E-E^{\theta'})} - C_R(0,t)e^{(1-\alpha)f(E-E^{\theta'})}\right] \tag{8}$$

in equation (8), f equals to $F/_{RT}$.

Combining boundary conditions of the above equations, and using finite element method to calculate equations (7) and (8), we can obtain

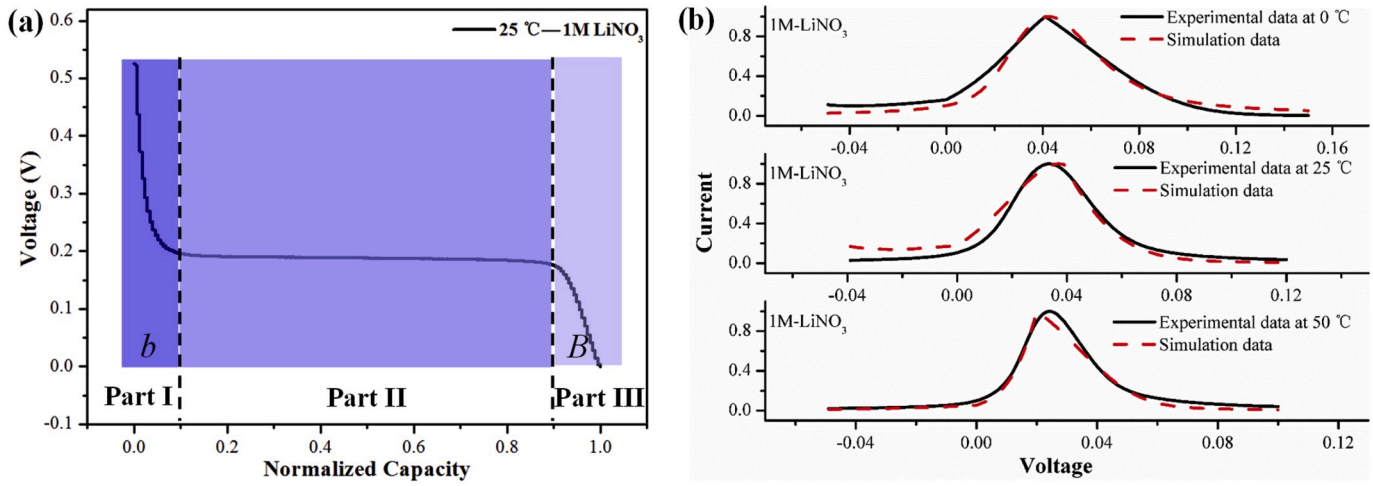

Fig. 2. (a) The normalized discharge curve of QSP electrode measured in 1 M $LiNO_3$, which was divided into three parts for convenience of simulation. (b) The CV curves of QSP electrode tested in 1 M $LiNO_3$ at different temperature, the dotted lines are the simulation curves by the updated SP-model.

Li-ion kinetic parameters both in bulk and surface.

As shown in Fig. 1e, f and S6, $LiFePO_4$ QSP electrodes presented different electrochemical behaviors in 1 M $LiNO_3$, 1 M LiCl, 0.5 M Li_2SO_4, or 1 M CH_3COOLi at different temperatures. We simulated the testing data by the modified SP-model through changing the parameter of k^0, α, D_{Li} and E in this model, good fitting results were obtained, as shown in Fig. 2b and S9. The simulation results of k^0 are shown in Fig. 3a and b k^0 increases with the increase of testing temperature and k^0 at charge (Li-ion de-intercalation) is smaller about 60% than that at discharge (Li-ion intercalation), and this trend exists in all four kinds of electrolytes. However, at a certain temperature, the exact values of k^0 are different in the four kinds of electrolytes. The rate constant k^0 in $LiNO_3$ and LiCl solution are higher than in Li_2SO_4 and CH_3COOLi. In order to facilitate comparing the differences, the electrolytes were divided into two types: the fast-type ($LiNO_3$ and LiCl) and the slow-type (Li_2SO_4 and CH_3COOLi) according to the simulated data of k^0. k^0 in the fast-type is larger than that in the slow-type (Fig. 3a and b). We calculated E_a and A by interface kinetic Arrhenius equation ($\ln k^0 = \ln A\text{-}E_a/$

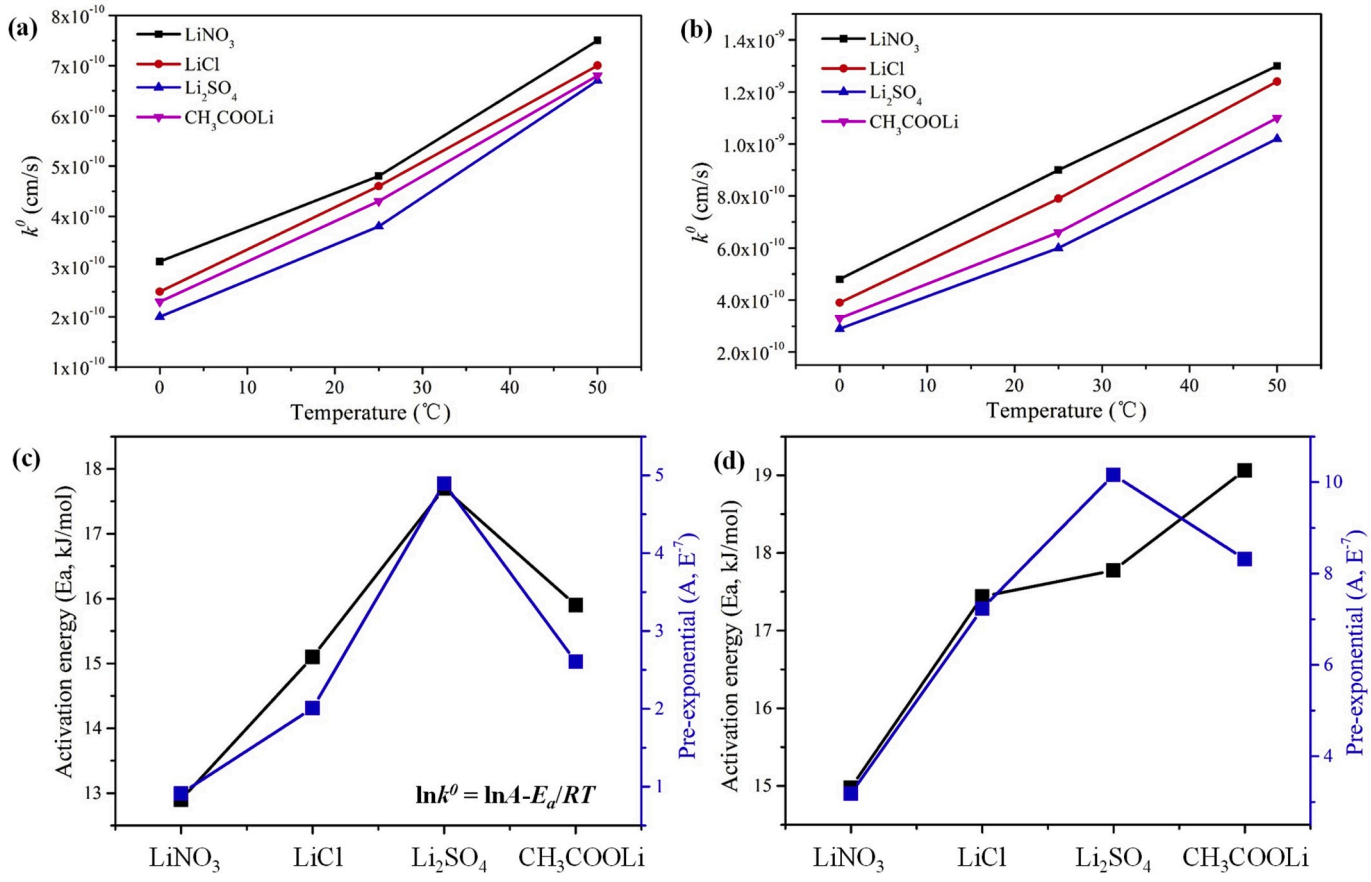

Fig. 3. The relationship between standard rate constant (k^0) and temperature (T) in different electrolytes during (a) charge and (b) discharge processes. Activation energy (E_a) and pre-exponential (A) of $LiFePO_4$ in different electrolytes, calculated by Arrhenius equation during (c) charge and (d) discharge processes.

RT, k^0 is the rate constant, E_a is activation energy, A is pre-exponential factor, R is molar gas constant, T is thermodynamic temperature), and the final results were shown in Fig. 3c and d. The detailed simulation processes and data of E_a and A were listed in Figs. S10 and S11. Obviously, the fast-type electrolytes owns smaller E_a and A compared with the slow-type electrolytes for Li-ion transport, indicating that the shorter jump distance and lower energy for Li-ion transport across the interface between electrolyte and electrode. Thus, our electrochemical simulations proved that the different polarizations in aqueous electrolytes with different salts indeed come from the different Helmholtz layer formed between $LiFePO_4$ and different aqueous electrolytes, leading to different activation energies and jump distances for Li-ion transport across the Helmholtz layer.

3.3. Section III. Density functional theory (DFT) calculation

In order to get an atomic cognition of the Helmholtz layer between $LiFePO_4$ and different aqueous electrolytes, a broader DFT study was carried out to explore the coordination environment of anions on the surface of $LiFePO_4$ and $FePO_4$. The interaction between the surface and the adsorbed species were calculated using basic ion pair model, Slab$-A^{n-} - nLi^+$ model, where A^{n-} represents the anions adsorbed (Cl^-, NO_3^-, CH_3COO^- and SO_4^{2-}). In the Slab $- A^{n-} - nLi^+$ model, the A^{n-} was allowed to relax on the slab and the Li^+ was fixed in the vacuum [5]. The binding energy (ΔE_b) was defined as follows:

$$\Delta E_b = E(i^*) - E(*) - E(i)$$

where $E(i^*)$ and $E(*)$ is the energy of the adsorption model and pristine surface respectively, and $E(i)$ is the energy of ion pair i ($A^{n-} - nLi^+$) or neutral molecule (H_2O). The geometrical structures and binding energies of these interactions are summarized in Fig. 4. Fig. 4a and g shows the pristine (010) surface of $FePO_4$ and $LiFePO_4$, which is an incomplete FeO_6-octahedral structure (to become FeO_5), in which one "O-atom" is missed due to symmetric breaking from 3D bulk crystal to 2D surface. The O-atom of H_2O and anions (or Cl^-) can place the missed "O-atom" on the surface of $FePO_4$/$LiFePO_4$ (010), and formed stable reconstructed octahedral structure as shown in Fig. 4a–l. According to our previous work, the detailed interface structure built by H_2O on the surface of $LiFePO_4$ and $FePO_4$ are shown in Figure 4m and n. Generally, the $LiFePO_4$ slab affords a much larger binding energy towards ions than $FePO_4$. The large binding energies of anions are induced by the as-

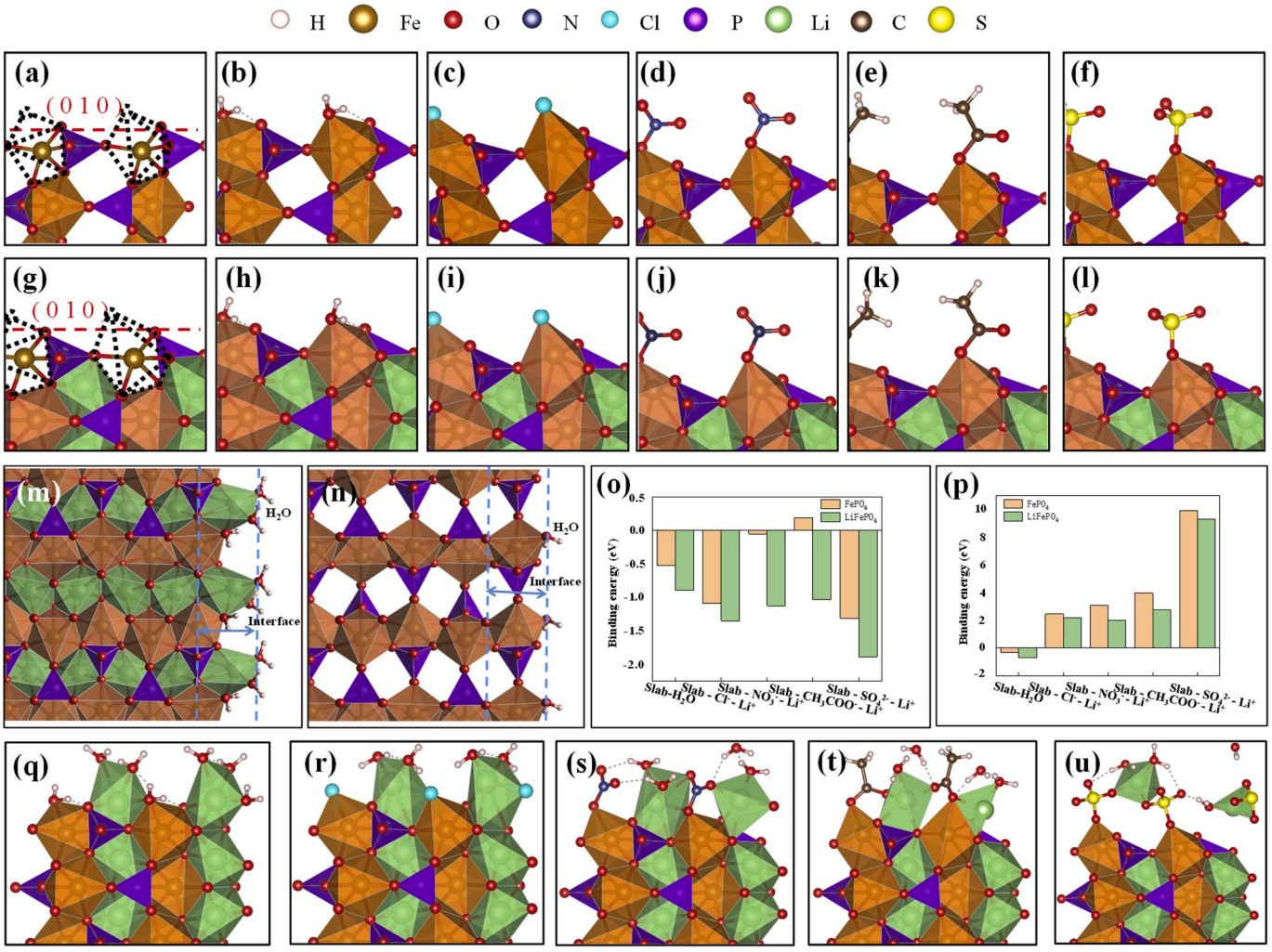

Fig. 4. (a) The structure of (0 1 0) surface of $FePO_4$ with (b) H_2O adsorbed, (c) Cl^- adsorbed, (d) NO_3^- adsorbed, (e) CH_3COO^- adsorbed and (f) SO_4^{2-} adsorbed. (g) The structure of pristine (0 1 0) surface of $FePO_4$. The structure of (0 1 0) surface of $LiFePO_4$ with (h) H_2O adsorbed, (i) Cl^- adsorbed, (j) NO_3^- adsorbed, (k) CH_3COO^- adsorbed and (l) SO_4^{2-} adsorbed. (m, n) the detailed Janus solid–liquid interface structure of $LiFePO_4$ and $FePO_4$ built by H_2O. (o) The binding energies of the Slab-H_2O and Slab-Anion-Li^+ models of $FePO_4$ and $LiFePO_4$. (p) The binding energies with de-solvation energy taken into consideration of the Slab-H_2O and Slab-Anion-Li^+ models of $FePO_4$ and $LiFePO_4$. The structure of "Janus" solid-liquid interface reconstructed by $Li^+(H_2O)_2$ on (010) surface of $LiFePO_4$ with (q) H_2O, (r) Cl^-, (s) NO_3^-, (t) CH_3COO^- and (u) SO_4^{2-} adsorption.

formed strong Fe–O/Cl interactions as well as a significant charge transfer. It is obvious that some of Cl^-, NO_3^-, CH_3COO^- and SO_4^{2-} could bind with $LiFePO_4$ or $FePO_4$ slab spontaneously (Figure 4o). However, the interface reconstruction energy in different coordination environment are different with the influence of solvent water taken into consideration. The binding energy (ΔE_b) includes de-solvation energy ($E_{i,desol}$) were defined as follows:

$$\Delta E_b = E(i^*) - E(*) - (E(i) - E_{i,desol})$$

With $E_{i,desol}$ of H_2O and anions [27,28] taken into consideration, the ΔE_b of Cl^-, NO_3^-, CH_3COO^- and SO_4^{2-} all turn into positive (1.99–9.92 eV, Figure 4p). The results illustrate that it's a spontaneous process for H_2O to finish the octahedral interface reconstruction with Fe, as for the four kinds of anions, need external influence to construct perfect Janus-interface. So, in the aqueous electrolyte system, H_2O has absolute advantage to achieve interface reconstruction compared with the mentioned anions. The detailed Janus interface forming mechanism and interface charge transfer processes were shown in Fig. S12. Li-ions ($Li^+(H_2O)_4$) diffusion processes on the surface of $FePO_4$ needs to detach two water molecules to come to the surface owning to the Janus solid–liquid interface [8]. The structure of Janus solid-liquid interface built by ($Li^+(H_2O)_2$) on (010) surface of $LiFePO_4$ with H_2O, Cl^-, NO_3^-, CH_3CCO^- and SO_4^{2-} adsorption were shown in Fig. 4q–u. According to this, we calculated the energy changing curve of Li-ion embedding using the climbing image nudged elastic band method [29]. The migration energy barriers of Li-ion transfer from surface to bulk in different electrolytes under vacuum condition are different as shown in Fig. 4q–u, which are 0.27 eV (H_2O), 0.90 eV (Cl^-), 0.84 eV (NO_3^-), 0.94 eV (CH_3COO^-), and 1.01 eV (SO_4^{2-}). That's to say, anion diversity has a big influence on Li-ion solvation-desolvation process in vacuum environment.

Combine with the above calculation and analysis, obviously, in aqueous electrolyte H_2O will connect with Fe and form Fe–O octahedral structure and Janus interface (Fig. 5a). Obviously, the EDL on the surface of $FePO_4$ or $LiFePO_4$ includes Janus interface, anion absorption layer and cation absorption layer as shown in Fig. 5a, which has been described by Newman and Thomas-Alyea [3]. There is only one kind of cation in the above electrolytes, which is Li-ion, so the cation adsorption layer in the four kinds of interfaces should be the same. Hence, the difference of CV curves in different aqueous electrolytes must come from anions. The ionic radius and charge quantity of NO_3^-, Cl^-, SO_4^{2-}, and CH_3COO^- are different, which are 1.79 Å for Cl^-, 1.84 Å for NO_3^-, 1.62 Å for CH_3COO^- and 2.58 Å for SO_4^{2-}, so the size of the anions group (connected with H_2O) are different. The bigger of the anion group, the higher of activation energy for Li-ion realizing solvation-desolvation processes, because Li-ion needs a longer jump distance from electrolyte to the Janus interface (d in Fig. 5a). As for CH_3COO^-, owns a small radius but needs higher Li-ion activation energy, which can be indexed to the strong appetency with Li-ion (weak electrolyte). This should be the reason why the interfacial rate constant (k^0) and Ea in different electrolytes are different. Actually, the reconstruction layer and absorbed layer were belonged to Helmholtz Plane, and named as IHP and OHP as shown in Fig. 5b. IHP includes adsorbed molecules (Janus interface) and ions (anion adsorption layer), while solvated adsorbed ions (cation adsorption layer) are located in OHP. E_0, E_1 and E_2 represent the activation energies related to IHP (E_0+E_1) and OHP (E_2), and the summation of E_0, E_1 and E_2 equals to activation energy E_a shown in Fig. 3c and d. Herein, owing to the spontaneously reconstruction process between H_2O and $FePO_4$, the value of E_0 in the four electrolytes should be the same. Moreover, E_2 should be the same in the four kinds of interfaces, because of the single kind of cation. So the difference of E_a can be attributed to the difference of E_1 (anion adsorption layer), which owns the same variation trend compared with E_a as shown in Fig. 5b. Hence, it's easier for Li-ion passing through the Helmholtz Plane in $LiNO_3$ and LiCl electrolytes compared with it in Li_2SO_4 and CH_3COOLi, owning to the small E1 in IHP.

4. Conclusions

In this work, we prepared SP electrode of $LiFePO_4$, and did CV testing in different aqueous electrolytes (1 M $LiNO_3$, 1 M LiCl, 0.5 M Li_2SO_4, and 1 M CH_3COOLi) and different temperatures. Interestingly, differences were found in the CV curves between the four electrolytes, especially when the testing temperature was decreased. Combining with the improved SP model, the accurate interfacial rate constant k^0 and activation energy E_a in the four kinds of electrolytes were obtained. Ab initio calculations proved that it's easier for H_2O realizing octahedral interface reconstruction compared with NO_3^-, Cl^-, SO_4^{2-} and CH_3COO^-, so the reconstruction interface (Janus interface with both $FeO_5(H_2O)$ and $LiO_3(H_2O)_3$ octahedral reconstructive structure units) in the four kinds of electrolytes are the same. The activation energy of Li-ion from electrolyte to electrode includes three parts, which are Janus interface (IHP), anion adsorption layer (IHP) and cation adsorption layer (OHP). Owing to the same Janus interface and cation adsorption layer, the difference of

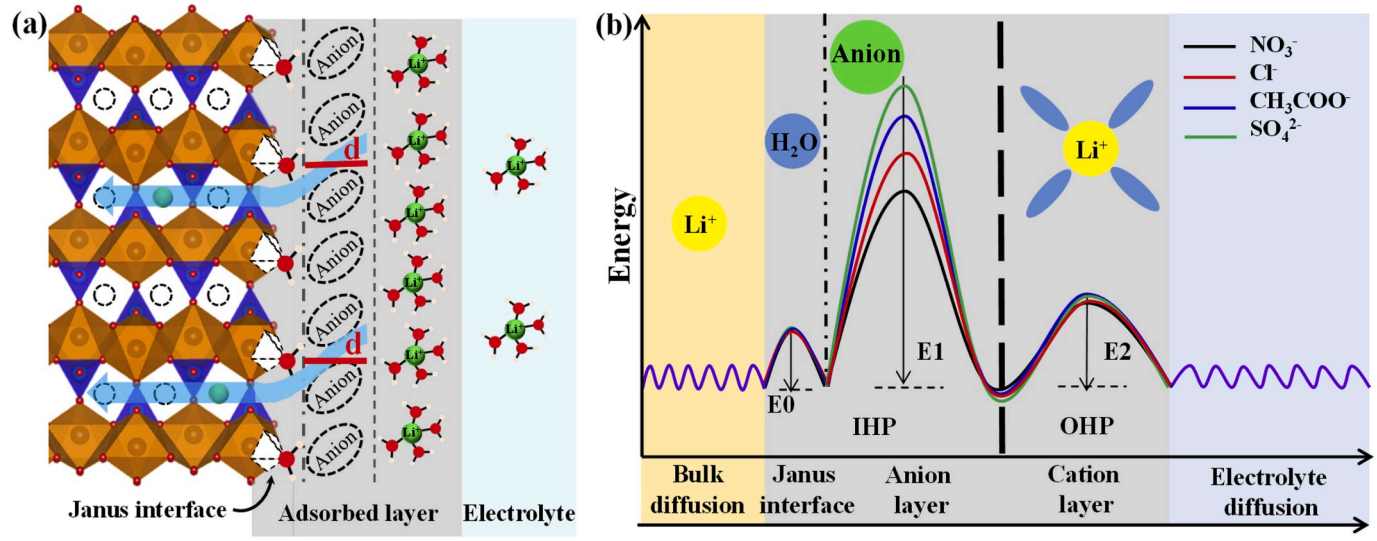

Fig. 5. (a) Schematic descriptions of the effect of anion on Li-ion transport from electrolyte to electrode. (b) The relationship of migration energy barrier of Li^+ with the inner Helmholtz plane (IHP) and outer Helmholtz plane (OHP).

E_a in the four kinds of electrolytes must come from the anion adsorption layer in IHP. This work provides a clear recognition about the role of anion on Li-ion transport at the electrode/electrolyte interface and a guiding significance on development of aqueous electrolyte systems.

Declaration of competing interest

The authors declare that they have no known competing financial interests or personal relationships that could have appeared to influence the work reported in this paper.

CRediT authorship contribution statement

Jiangtao Hu: Conceptualization, Investigation, Writing - original draft. **Wenju Ren:** Methodology. **Xin Chen:** Formal analysis. **Yiwei Li:** Investigation. **Weiyuan Huang:** Investigation. **Kai Yang:** Investigation. **Luyi Yang:** Investigation. **Yuan Lin:** Methodology. **Jiaxin Zheng:** Writing - review & editing. **Feng Pan:** Conceptualization, Writing - review & editing.

Acknowledgment

This work was financially supported by National Key R&D Program of China (2016YFB0700600), the National Natural Science Foundation of China (No. 21603007 and 51672012), and Shenzhen Science and Technology Research Grant (No. JCYJ20160531141048950, JCYJ20150729111733470).

Appendix A. Supplementary data

Supplementary data to this article can be found online at https://doi.org/10.1016/j.nanoen.2020.104864.

References

[1] J. Huang, Z. Li, H. Ge, J. Zhang, J. Electrochem. Soc. 162 (2015) A7037–A7048.
[2] T. Liu, L. Lin, X. Bi, L. Tian, K. Yang, J. Liu, M. Li, Z. Chen, J. Lu, K. Amine, K. Xu, F. Pan, Nat. Nanotechnol. 14 (2019) 50–56.
[3] J. Newman, K.E. Thomas-Alyea, Electrochemical Systems, John Wiley & Sons, Hoboken, NJ, 2004.
[4] O. Borodin, X. Ren, J. Vatamanu, A. von Wald Cresce, J. Knap, K. Xu, Acc. Chem. Res. 50 (2017) 2886–2894.
[5] C. Yan, H.R. Li, X. Chen, X.Q. Zhang, X.B. Cheng, R. Xu, J.Q. Huang, Q. Zhang, J. Am. Chem. Soc. 141 (2019) 9422–9429.
[6] C. Yang, J. Chen, T. Qing, X. Fan, W. Sun, A. von Cresce, M.S. Ding, O. Borodin, J. Vatamanu, M.A. Schroeder, N. Eidson, C. Wang, K. Xu, Joule 1 (2017) 122–132.
[7] L. Suo, O. Borodin, T. Gao, M. Olguin, J. Ho, X. Fan, C. Luo, C. Wang, K. Xu, Science 350 (2015) 938–943.
[8] J. Hu, W. Li, Y. Duan, S. Cui, X. Song, Y. Liu, J. Zheng, Y. Lin, F. Pan, Adv. Energy Mater. 7 (2017), 1601894.
[9] J. Zheng, Y. Hou, Y. Duan, X. Song, Y. Wei, T. Liu, J. Hu, H. Guo, Z. Zhuo, L. Liu, Z. Chang, X. Wang, D. Zherebetskyy, Y. Fang, Y. Lin, K. Xu, L.-W. Wang, Y. Wu, F. Pan, Nano Lett. 15 (2015) 6102–6109.
[10] X. Song, T. Liu, J. Amine, Y. Duan, J. Zheng, Y. Lin, F. Pan, Nano Energy 37 (2017) 90–97.
[11] P. Yan, J. Zheng, J. Liu, B. Wang, X. Cheng, Y. Zhang, X. Sun, C. Wang, J.-G. Zhang, Nat. Energy 3 (2018) 600–605.
[12] L.Z.Z. Liu, W. Zhao, J. Zheng, Y. Yang, G. Wang, J.-G. Zhang, C. Wang, Microsc. Microanal. 24 (2018) 1522–1523.
[13] K. Zaghib, M. Dontigny, P. Charest, J.F. Labrecque, A. Guerfi, M. Kopec, A. Mauger, F. Gendron, C.M. Julien, J. Power Sources 185 (2008) 698–710.
[14] Y. Li, H. Chen, K. Lim, H.D. Deng, J. Lim, D. Fraggedakis, P.M. Attia, S.C. Lee, N. Jin, J. Moskon, Z. Guan, W.E. Gent, J. Hong, Y.S. Yu, M. Gaberscek, M.S. Islam, M.Z. Bazant, W.C. Chueh, Nat. Mater. 17 (2018) 915–922.
[15] J.P. Perdew, K. Burke, M. Ernzerhof, Phys. Rev. Lett. 77 (1996) 3865–3868.
[16] G. Kresse, J. Furthmüller, Phys. Rev. B 54 (1996) 11169–11186.
[17] G. Kresse, Phys. Rev. B 59 (1999) 1758–1775.
[18] H.J. Monkhorst, J.D. Pack, Phys. Rev. B 13 (1976) 5188–5192.
[19] P.S. Herle, B. Ellis, N. Coombs, L.F. Nazar, Nat. Mater. 3 (2004) 147–152.
[20] C. Huang, D. Ai, L. Wang, X. He, Chem. Lett. 42 (2013) 1191–1193.
[21] J. Wang, J. Yang, Y. Zhang, Y. Li, Y. Tang, M.N. Banis, X. Li, G. Liang, R. Li, X. Sun, Adv. Funct. Mater. 23 (2013) 806–814.
[22] A.A. Salah, A. Mauger, C.M. Julien, F. Gendron, Mater. Sci. Eng. B 129 (2006) 232–244.
[23] Y. Duan, B. Zhang, J. Zheng, J. Hu, J. Wen, D.J. Miller, P. Yan, T. Liu, H. Guo, W. Li, X. Song, Z. Zhuo, C. Liu, H. Tang, R. Tan, Z. Chen, Y. Ren, Y. Lin, W. Yang, C.-M. Wang, L.-W. Wang, J. Lu, K. Amine, F. Pan, Nano Lett. 17 (2017) 6018–6026.
[24] L. Wang, X. He, W. Sun, J. Wang, Y. Li, S. Fan, Nano Lett. 12 (2012) 5632–5636.
[25] L. Wang, W. Sun, X. Tang, X. Huang, X. He, J. Li, Q. Zhang, J. Gao, G. Tian, S. Fan, J. Power Sources 244 (2013) 94–100.
[26] R. Amin, P. Balaya, J. Maier, Electrochem. Solid State Lett. 10 (2007) A13–A16.
[27] Y. Marcus, J. Chem. Soc. 87 (1991) 2995–2999.
[28] J.R. Pliego, J.M. Riveros, Chem. Phys. Lett. 332 (2000) 597–602.
[29] G. Henkelman, B.P. Uberuaga, H. Jónsson, J. Chem. Phys. 113 (2000) 9901–9904.